Ceramics International xxx (xxxx) xxx

Contents lists available at ScienceDirect

Ceramics International

journal homepage: www.elsevier.com/locate/ceramint

Enhancing thermoelectric performance of $CaMnO_3$ through a Y- and La-dual-doping strategy

P. Amirkhizi [a,*], M.A. Madre [b], O.J. Dura [c], M.A. Torres [b], A. Sotelo [b], A.V. Kovalevsky [a], Sh. Rasekh [a]

[a] Department of Materials and Ceramic Engineering, CICECO-Aveiro Institute of Materials, University of Aveiro, 3810-193, Aveiro, Portugal
[b] INMA (CSIC-Universidad de Zaragoza), M^a de Luna, 3, 50018, Zaragoza, Spain
[c] Applied Physics Department, University of Castilla-La Mancha, Ciudad Real, 13071, Spain

ARTICLE INFO

Handling Editor: P. Vincenzini

Keywords:
Calcium manganite
Thermoelectrics
Dual doping
Electrical properties
Thermal properties

ABSTRACT

A classical ceramic route has been used in this work to prepare Y and La co-doped $CaMnO_3$ thermoelectric compound seeking to improve its thermoelectric properties. The study highlights significant improvements in electrical and thermal transport properties achieved with minimal doping levels and a cost-effective synthesis process. The co-doping strategy effectively reduced electrical resistivity (reaching 10.8 mΩ cm at 800 °C for 0.03 (Y, La)-doped samples) while maintaining a relatively high Seebeck coefficient (300 μV/K at 800 °C for 0.01 (Y, La)-doped samples). Moreover, the thermal conductivity was minimized (1.65 W/(K m) at 800 °C for 0.03 (Y, La)-doped samples), leading to outstanding thermoelectric performance, with 0.47 mW/(K^2m) power factor, and 0.25 ZT values at 800 °C (for 0.01 (Y, La)-doped samples. These results are among the best values reported so far for this family of compounds, underscoring the potential of this material for high-temperature thermoelectric applications and the efficiency of the classical ceramic approach with reduced dopant usage.

1. Introduction

The impressive growth of the world's population and increase of energy demand associated with it led to a vital search for sustainable alternatives. Traditional energy sources not only contribute to environmental problems, but also exhibit low efficiency and cause the loss of a significant portion of energy as heat. Considering these issues, the exploration of green energy sources has become necessary to replace traditional sources [1–3].

Thermoelectric materials, which are able to convert waste heat directly into electricity, have emerged as a promising way to recover energy. The efficiency of this conversion is normally defined using the dimensionless figure of merit ZT, equal to $ZT = S^2\sigma T/\kappa$ where $S^2\sigma$ is known as the power factor, PF, and represents the capability of electrical energy production; in these expressions, S, σ, κ and T are the Seebeck coefficient (or thermopower), electrical conductivity, total thermal conductivity and absolute temperature, respectively [4]. For example, Bismuth Telluride (Bi_2Te_3) is a well-known thermoelectric material that exhibits a high ZT value at room temperature, making it suitable for applications in power generation and refrigeration [5,6]. Another example is Lead Telluride (PbTe), which has been extensively studied for the mid-temperature range applications due to its favorable thermoelectric properties [7,8]. While important steps have been taken in this area since the 1960s, some challenges still remain, such as optimizing material properties for specific temperature ranges and improving the overall efficiency of thermoelectric devices [9]. Classical thermoelectric materials, which are currently commercialized, possess two major issues: they are composed of heavy, toxic, and rare elements, which make them expensive and environmentally incompatible. Moreover, their application at high temperatures is limited due to evaporation, degradation, and oxidation, etc. [10].

In the search for environmentally friendly alternatives, ceramic oxides have gained attention since the discovery of promising thermoelectric properties in $NaCo_2O_4$ [11], due to their high-temperature stability, relative abundance, and affordability. Among ceramic oxides, $CaMnO_3$, a perovskite-type oxide, has attracted the attention of researchers due to its remarkable thermoelectric properties, particularly high Seebeck coefficient and relatively low thermal conductivity.

* Corresponding author. Department of Materials and Ceramic Engineering, CICECO-Aveiro Institute of Materials, University of Aveiro, 3810-193, Aveiro, Portugal.
E-mail address: parisa.amirkhizi@ua.pt (P. Amirkhizi).

https://doi.org/10.1016/j.ceramint.2024.12.375
Received 9 September 2024; Received in revised form 13 December 2024; Accepted 21 December 2024
Available online 23 December 2024

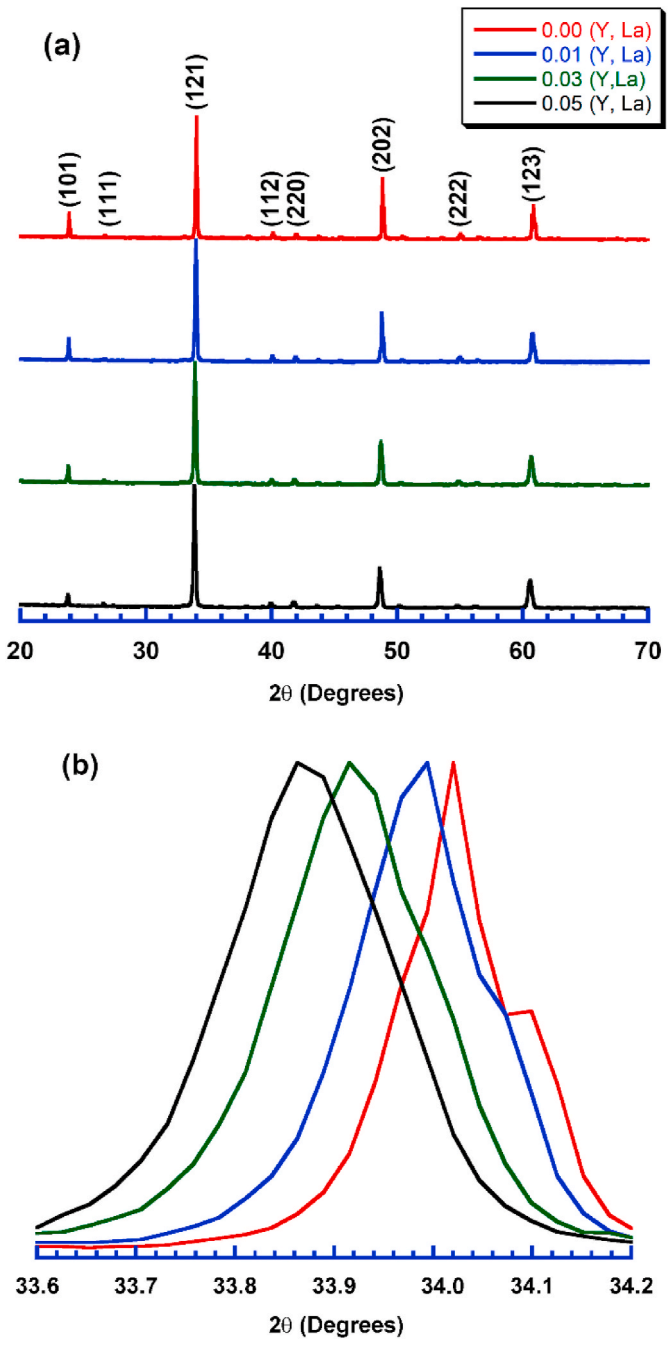

Fig. 1. a) Powder XRD patterns of all sintered samples. The diffraction planes identify the peaks associated with the $CaMnO_3$ phase; b) enlarged view of the 34° peak showing the shift towards a lower angle when the amount of dopant is higher.

Moreover, this material can be prepared directly in air, avoiding the necessity to use a vacuum, inert or reducing atmospheres, as it is required for many other families of thermoelectric materials. However, achieving a high figure of merit (ZT) remains a challenge. To overcome this barrier, researchers have explored various strategies, including doping with different elements to optimize electrical conductivity and charge carrier concentration [12–17].

This work focuses on improving the thermoelectric performance of $CaMnO_3$ by introducing Y and La elements as dopants in the Ca-site, due to their lower cost compared to other rare earths typically used for $CaMnO_3$ doping. The chosen composition, $Ca_{1-2x}Y_xLa_xMnO_3$ (x = 0, 0.01, 0.03, and 0.05), building upon our previous research with single doping of these elements, aims to further optimize the material's electrical conductivity and its ability to scatter phonons of different wavelengths, which are crucial for improved thermoelectric performance. The success of this approach will be evaluated by closely examining the thermoelectric properties of the final sintered materials and linking them to the structural and microstructural characteristics. Through proposed dual-doping strategy and addressing the challenges associated with $CaMnO_3$, this research aims to contribute to the ongoing efforts in advancing sustainable and efficient thermoelectric materials.

2. Experimental procedure

The initial $Ca_{1-2x}Y_xLa_xMnO_3$ compositions (x = 0, 0.01, 0.03, and 0.05) used in this research were prepared from $CaCO_3$ (≥98 %, Pan-Reac), Y_2O_3 (99.99 %, Sigma), La_2O_3 (99 %, Panreac), and Mn_2O_3 (99 %, Aldrich) commercial powders. The precursor powders were weighed in the appropriate proportions and ball-milled in water media for 30 min at 300 rpm. The homogeneous ball-milled compositions were then dried under infrared radiation until total water evaporation and manually milled before being placed into a furnace for two-steps calcination, at 950 °C and 1050 °C for 12 h under air atmosphere, with an intermediate manual milling to promote solid-state reaction and decompose the carbonates. All resulting powders were cold uniaxially pressed in the form of pellets (3 x 3 × 15 mm^3) under 400 MPa while using PVA as binder. To remove the PVA, the pellets were placed into a furnace at 450 °C for 2 h, followed by sintering at 1310 °C for 12 h at 3 °C/min heating rate, and cooled to room temperature at 5 °C/min.

Phase identification in the sintered materials has been performed by powder X-Ray Diffraction (XRD) analysis at room temperature, using a PHILIPS X'PERT system with CuK_α radiation (λ = 1.5406 Å), with 2θ ranging between 20 and 75°. Unit cell parameters were calculated using FullProf software (Rietveld refinement) from the XRD recorded data. Morphological and microstructural characterization of samples surface was performed using field emission scanning electron microscopy (FESEM, Zeiss Merlin) complemented by energy-dispersive spectrometry (EDS) for elemental analysis. The density of samples was measured through the well-known Archimedes' method for several sintered samples of each composition to minimize measurement errors. X-ray photoelectron spectroscopy (XPS) measurements on selected samples were collected using a Flexps Specs photoelectron spectrometer with Al Kα (1486.7 eV) radiation. The binding energies were calibrated by utilizing the C 1s peak (284.4 eV) as reference. Powdered samples were placed on carbon tape and measurement is done at UV. Deconvolution of the Mn 2p was done by fitting voigt functions within the SpecsLab

Table 1
Lattice parameters as a function of the dopant content, as well as the vol. % of $CaMn_2O_4$ secondary phase, obtained from the XRD data along with reliability factors.

Composition	a (Å)	B (Å)	c (Å)	Vol. %	Reliability factors			
$Ca_{1-2x}Y_xLa_xMnO_3$				$CaMn_2O_4$	Rp	Rwp	Rexp	Chi2
x = 0.00	*5.28262 (0.00015)*	*7.45673 (0.00020)*	*5.26758 (0.00014)*	*10.21*	*5.71*	*7.74*	*3.79*	*4.17*
x = 0.01	*5.28560 (0.00024)*	*7.46009 (0.00033)*	*5.27168 (0.00022)*	*8.76*	*5.00*	*6.42*	*3.78*	*2.88*
x = 0.03	*5.29484 (0.00028)*	*7.47103 (0.00038)*	*5.27959 (0.00026)*	*7.21*	*4.01*	*5.13*	*3.62*	*2.01*
x = 0.05	*5.30402 (0.00031)*	*7.48199 (0.00042)*	*5.28706 (0.00028)*	*8.34*	*4.03*	*5.05*	*3.51*	*2.07*

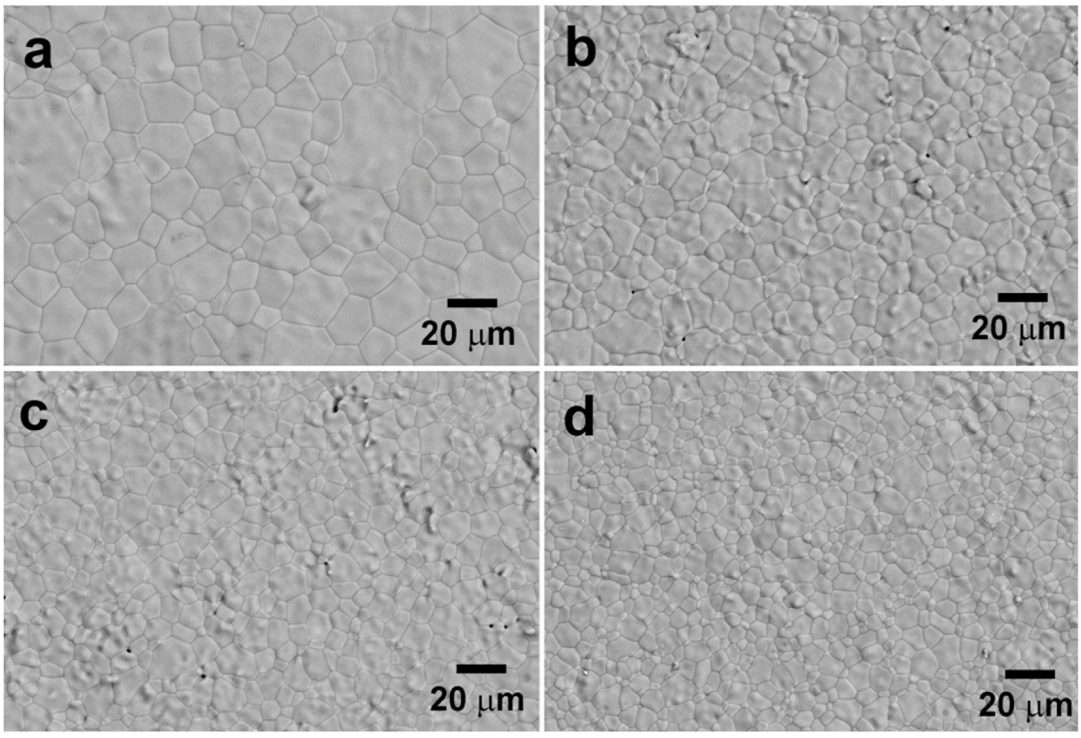

Fig. 2. Representative SEM images taken with backscattered electrons on the surfaces of $Ca_{1-2x}Y_xLa_xMnO_3$ samples, for x = a) 0.0; b) 0.01; c) 0.03; and d) 0.05.

Table 2
Absolute density values, with their standard error, determined by the Archimedes' method, and mean grain size, together with their standard error.

Composition $Ca_{1-2x}Y_xLa_xMnO_3$	Density (g/cm^3)	Std. Error (g/cm^3)	Mean grain size (μm)	Std. Error (μm)
X = 0.00	4.03	0.08	12.81	0.26
X = 0.01	4.00	0.05	8.05	0.20
X = 0.03	4.31	0.07	6.85	0.28
X = 0.05	4.39	0.10	4.78	0.15

Prodigy software to the experimental data using the Shirley baseline model.

Both electrical resistivity and Seebeck coefficient values of all samples were simultaneously measured, utilizing the standard DC four-probe technique, in an LSR-3 apparatus (Linseis GmbH) between 50 and 800 °C (in He atmosphere) under steady-state conditions. From the measured S and ρ values, the PF ($=S^2/\rho$) values were calculated to determine the electrical performances of samples. The total thermal conductivity (κ) was calculated using the formula $\kappa = \alpha\ C_p\ d$, where α represents thermal diffusivity, C_p specific heat, and d density of the sample. Thermal diffusivity (α) was determined using a laser-flash system (Linseis LFA 1000) operating between 50 and 800 °C. Specific heat (C_p) was calculated employing the Dulong-Petit law. Subsequently, the ZT (figure of merit) evolution with temperature was determined using both electrical and thermal data and compared with the data documented in the literature for this group of compounds.

3. Results and discussion

The powder XRD patterns are depicted for all samples in Fig. 1a covering the range from 20 to 70° for clarity. The graph clearly indicates that the most prominent peaks, denoted by their diffraction planes, are associated with *Pnma* space group $CaMnO_3$ phase, which is consistent with previous reported data [18,19]. Furthermore, the sharp peaks indicate a well-crystallized polycrystalline structure. Moreover, the nearly single-phase nature of all samples is evident, attributed to the high reactivity of precursors resulting from small particle sizes. On the other hand, it is also clear that Y and La are incorporated into the crystal structure, as no (Y,La)-based secondary phases have been identified. This result is further confirmed in Fig. 1b, which provides an enlarged view of the 34° peak for all samples, where a noticeable peak shift towards lower angles is observed when Y and La content is increased, indicating the incorporation of the dopants into the crystal structure of $CaMnO_3$.

To assess the effect of doping on the evolution of cell parameters, Rietveld refinement was conducted for each sample, using *Pnma* space group (62) as undoped $CaMnO_3$. The results obtained for the cell parameters for all samples, along with their respective errors and reliability factors with all non-excluded points for pattern, are summarized in Table 1. As it is shown in the table, cell parameters gradually increase with higher Y and La content, due to the increase of oxygen content in the structure provided by the higher oxidation state of Y, and La, when compared to that of Ca. Furthermore, the doped samples exhibit slightly lower content of the $CaMn_2O_4$ secondary phase than the undoped one.

Fig. 2 shows typical SEM micrographs of the samples surfaces after sintering, using backscattered electrons. In these images a very small amount of porosity can be found, independently of the dopant content. To verify these observations, sample density was measured using Archimedes' method, and the results are listed in Table 2. These data clearly confirm the SEM observations. Notably, these values correspond to relative densities between 86 % and 89 % of the theoretical density for the $CaMnO_3$ compound, which is comparable to the typical reported ones for this compound family [20–24]. Additionally, in the micrographs it is observed that the grain sizes decrease as the dopant level increases, suggesting that dopants inhibit grain growth and prevent the coarsening phenomenon. This trend was confirmed by measuring the mean grain size and their standard errors across several micrographs using the line intercept method [25], presenting these data in Table 2. In spite of the regular variation of mean grain size, another notable aspect observed in the micrographs is the large grain size variability due to

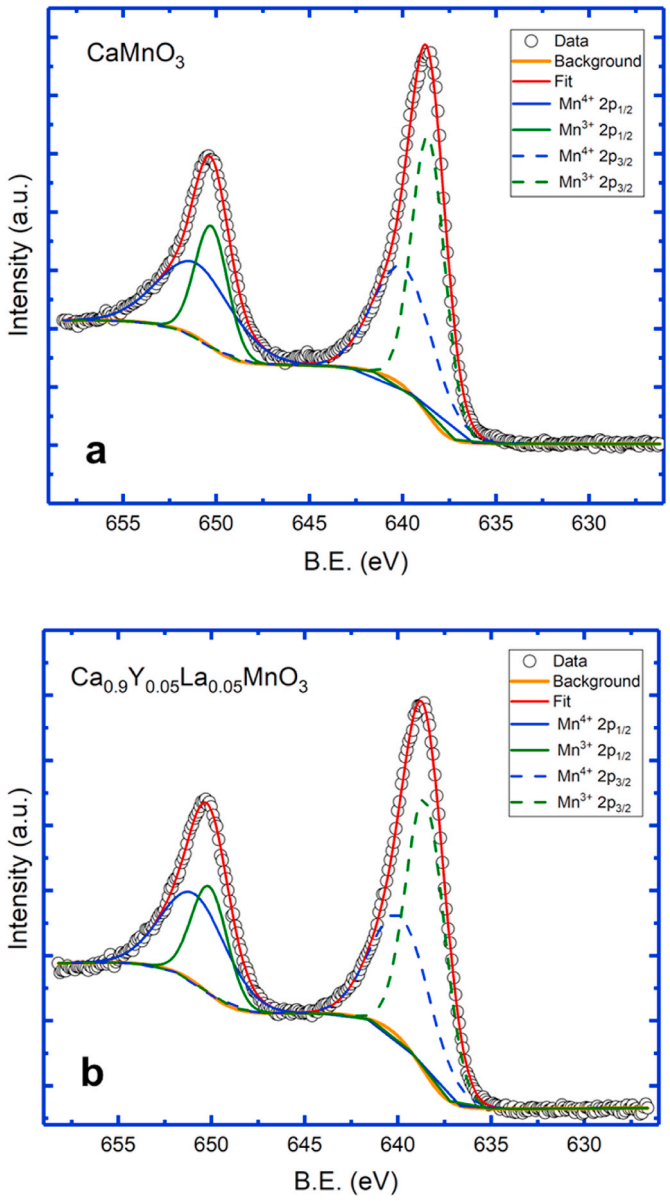

Fig. 3. Mn 2p XPS spectra for the $CaMnO_3$ (a) and $Ca_{0.9}Y_{0.05}La_{0.05}MnO_3$ (b) samples. Solid lines correspond to the analyses described in the text whereas points correspond to the experimental data.

uneven grain growth in these samples. These morphological changes are generally attributed to high calcination temperatures and extended sintering durations. Moreover, although the $CaMn_2O_4$ phase was identified in the XRD refinement, these images only show the presence of one phase (only one contrast can be identified). This fact can be explained based on prior studies indicating that this secondary phase could be found as intergrowths within the thermoelectric grains [26].

In order to evaluate the oxygen content in samples with different composition we preformed XPS analysis to measure the Mn oxidation state. Fig. 3 shows the XPS spectra of the Mn 2p levels in $CaMnO_3$ and $Ca_{0.9}Y_{0.05}La_{0.05}MnO_3$. Both characteristics peaks, $2p_{1/2}$ and $2p_{3/2}$, splits into two peaks related to the binding energies of Mn^{4+} and Mn^{3+}. In both samples, the $2p_{1/2}$ peak splits into two peaks at 651.0 ± 0.1 and 650.0 ± 0.1 eV corresponding to the Mn^{4+} and Mn^{3+}, respectively. In the case of the $2p_{3/2}$ this peak splits into 639.8 ± 0.1 and 638.8 ± 0.1 eV which also correspond to the Mn^{4+} and Mn^{3+} binding energies, respectively. This confirms a mixed chemical state and allows estimation of the Mn^{4+}/Mn^{3+} ratio in the two analysed samples. For $CaMnO_3$ the

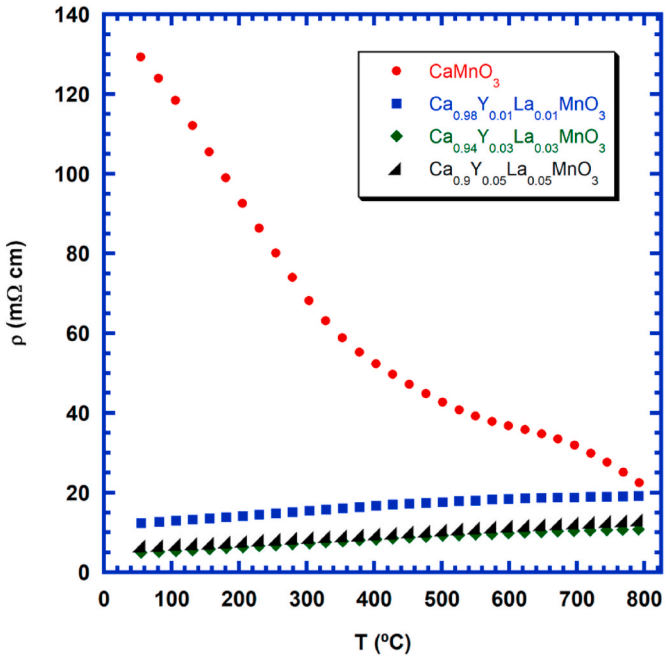

Fig. 4. Electrical resistivity variation with temperature as a function of the dopant content.

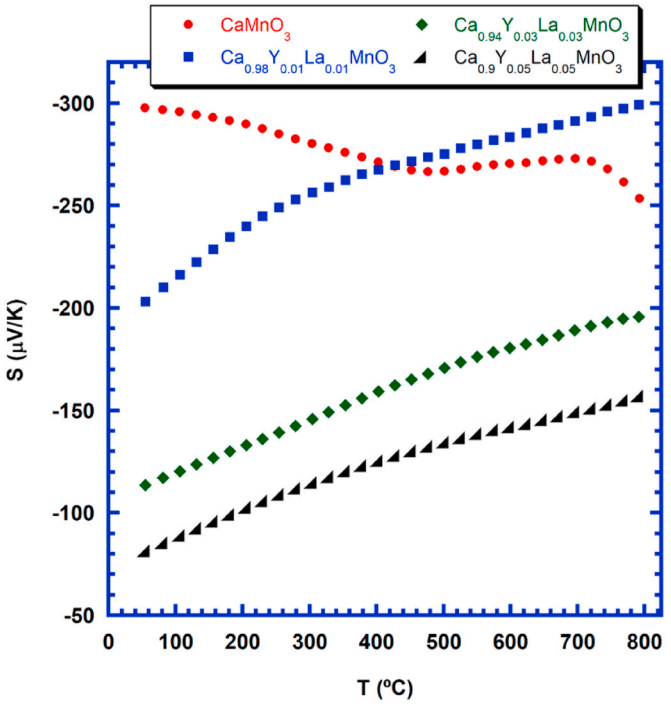

Fig. 5. Seebeck coefficient variation with temperature as a function of the dopant content.

Mn^{4+}/Mn^{3+} ratio is 0.98, whereas for $Ca_{0.9}Y_{0.05}La_{0.05}MnO_3$ it is 0.92, indicating a slightly lower presence of Mn^{4+} in the doped sample. Since a higher oxidation state of Mn implies more oxygen atoms in the atomic structure, the presence of Mn^{3+} indicates an oxygen deficiency, which is usually present in $CaMnO_3$ [27,28]. On the other hand, the lower Mn^{4+}/Mn^{3+} ratio obtained in the doped sample ($x = 0.05$) is related to the higher oxidation state of dopants (La^{3+} and Y^{3+}) and rules out the incorporation of oxygen defects due to chemical substitution.

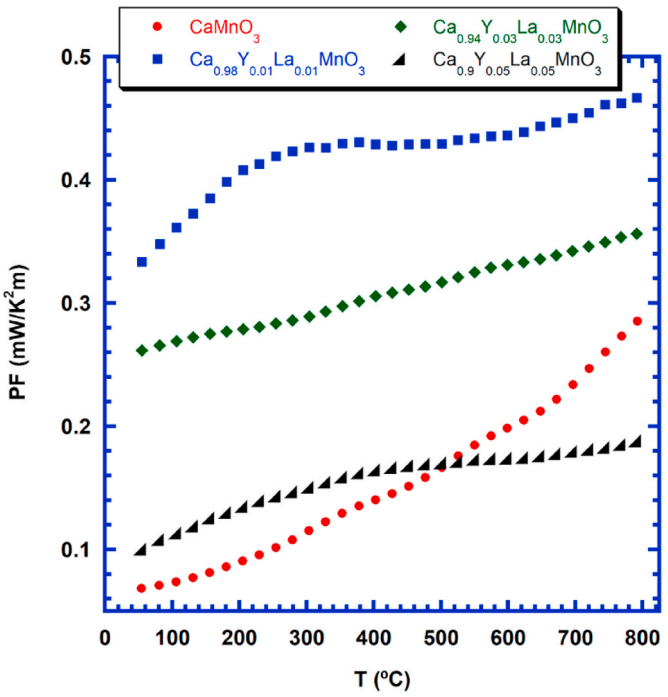

Fig. 6. Power factor variation with temperature as a function of the dopant content.

Consequently, the oxygen content in the samples is, approximately, the same independently of the dopant proportion, around 2.75.

Fig. 4 illustrates the evolution of electrical resistivity with temperature as a function of the dopant content. As it can be observed, all doped samples display lower electrical resistivity than the undoped one in the whole measured temperature range. This difference is due to the increase of charge carrier concentration resulted from partial substitution of Ca^{2+} cation by Y^{3+} and La^{3+}. Moreover, the values decrease with the dopant content up to 0.03, slightly increasing for higher substitution. This evolution clearly reflects the effect of other factors on the electrical resistivity, such as the decrease in grain size which can lead to increased grain boundary scattering and the increase in the number of defects in the samples such as vacancies and interstitials, which can scatter charge carriers and hinder their movement. These factors tend to increase the electrical resistivity and, consequently, the measured values reflect a compromise between those factors and the increase in the charge carrier concentration. These facts clearly explain that electrical resistivity is firstly drastically decreased for low dopant content when compared to the undoped samples, while increasing the Ca-substitution, the decrease is much lower, and increases for the highest dopant content. Another important effect induced by doping in these samples is the drastic change of behavior, being semiconducting-like ($d\rho/dT < 0$) for the undoped sample, in agreement with previously published data [29,30], while it is metallic-like ($d\rho/dT > 0$) for all doped ones. The lowest resistivity at 800 °C has been measured in samples with $x = 0.03$ (10.8 mΩ cm), which is in the order of the typically reported in this family of materials (8–12 mΩ cm) [13,16,31–35]. On the other hand, it is still higher than the best found in the literature for co-doped compounds (3.6–6.5 mΩ cm) [36–38].

Fig. 5 displays the evolution of the Seebeck coefficient with temperature for all samples. As it can be seen in the plot, all values are negative in the whole measured temperature range, indicating n-type behavior and that major charge carriers are electrons. Moreover, |S| increases with temperature in all doped samples, which is in agreement with the behavior of metals or degenerate semiconductor materials when their carrier concentration, effective mass, and Fermi level variation with temperature is negligible [39]. Additionally, the values of |S| are monotonically decreasing when the amount of dopant is raised, reflecting the higher charge carrier concentration, as it is much less sensitive to the other factors affecting the electrical resistivity previously discussed. The highest |S| values obtained within the doped samples (~300 μV/K) at 800 °C have been measured in 0.01(Y,La)-doped samples, which is about 50 % higher than those determined in 0.03(Y,La)-doped ones prepared in this work. Furthermore, they are much higher than the typically reported for doped $CaMnO_3$ (95–160 μV/K) [13,16,31–38].

Fig. 6 presents the evolution of PF with temperature for all samples, calculated from the electrical resistivity and Seebeck coefficient data. As it can be observed in the graph, all doped samples display higher PF values than the undoped one, except for the 0.05(Y,La)-doped samples at $T > 500$ °C due to their very low |S| values. Despite the fact that the 0.01(Y,La)-doped samples do not present the lowest electrical resistivity values, they reach the highest PF value at 800 °C (~0.47 mW/K^2m) provided by their very high |S| values. This value is around 30 % higher than that determined in 0.03(Y,La)-doped samples, and higher than those reported in the literature (0.1–0.4 mW/K^2m) [13,16,31–38,40,41].

Fig. 7 illustrates the electronic, phononic and the total thermal conductivity (κ_{el}, κ_{ph} and κ, respectively) variation with temperature for all samples. As it can be observed in Fig. 7c, κ decreases with temperature in all cases, in agreement with previously published results [36,38,39]. Moreover, in spite of the increased charge carrier concentration, which leads to a rise in electronic thermal conductivity (Fig. 7a), it is reduced when the amount of dopant is increased. This evolution is due to the phonon scattering associated to the decrease of the grain sizes (increase in the number of grain boundaries), and the substitution of Ca with much higher atomic weight cations. Consequently, the lowest κ at 800 °C has been found in 0.05(Y,La)-doped samples (1.65 W/K m), which is about 50 % lower than that of the undoped sample. Additionally, it is among the best ones reported in the literature for electron-doped $CaMnO_3$ compounds (1.4–3.6 W/K m) [33,40–44]. In addition, the phononic thermal conductivity displays the same behavior found for the total one in all samples. This fact can be associated with a more important effect of the dopants and the grain boundaries on the phonon scattering, than that produced by the increase of charge carrier concentration.

Fig. 8 presents the ZT evolution with temperature for all samples, calculated from the electrical resistivity, Seebeck coefficient and thermal conductivity data. It can be clearly observed the higher ZT values of all doped samples when compared to the undoped one in the whole measured temperature range. Moreover, the highest values are achieved for 0.01(Y,La)-doped samples due to their very high Seebeck coefficient and moderate electrical resistivity and thermal conductivity. The highest ZT value determined in these samples at 800 °C (~0.25) is around 177 % higher than that of the sample without any dopants. It is worth mentioning that the obtained ZT is among the best results reported in the literature in which more complex and longer processes, together with larger amounts of more expensive rare earths (0.08–0.29), were used [26,33,41,42,44–48].

It should be highlighted the fact that the high ZT values obtained in this work have been obtained through the classical ceramic method, much shorter and simpler than most of the methods used in the literature. Moreover, the best values have been achieved with a very small amount of dopants, and much cheaper than those used in the relevant bibliography.

4. Conclusions

In this work, the use of small amounts and relatively low-cost dopants on $CaMnO_3$ thermoelectric compound prepared through the classical solid-state method was studied, seeking the improvement of its thermoelectric properties. Powder XRD patterns showed the formation of doped-$CaMnO_3$ phase as the major one in all cases, with an increase of

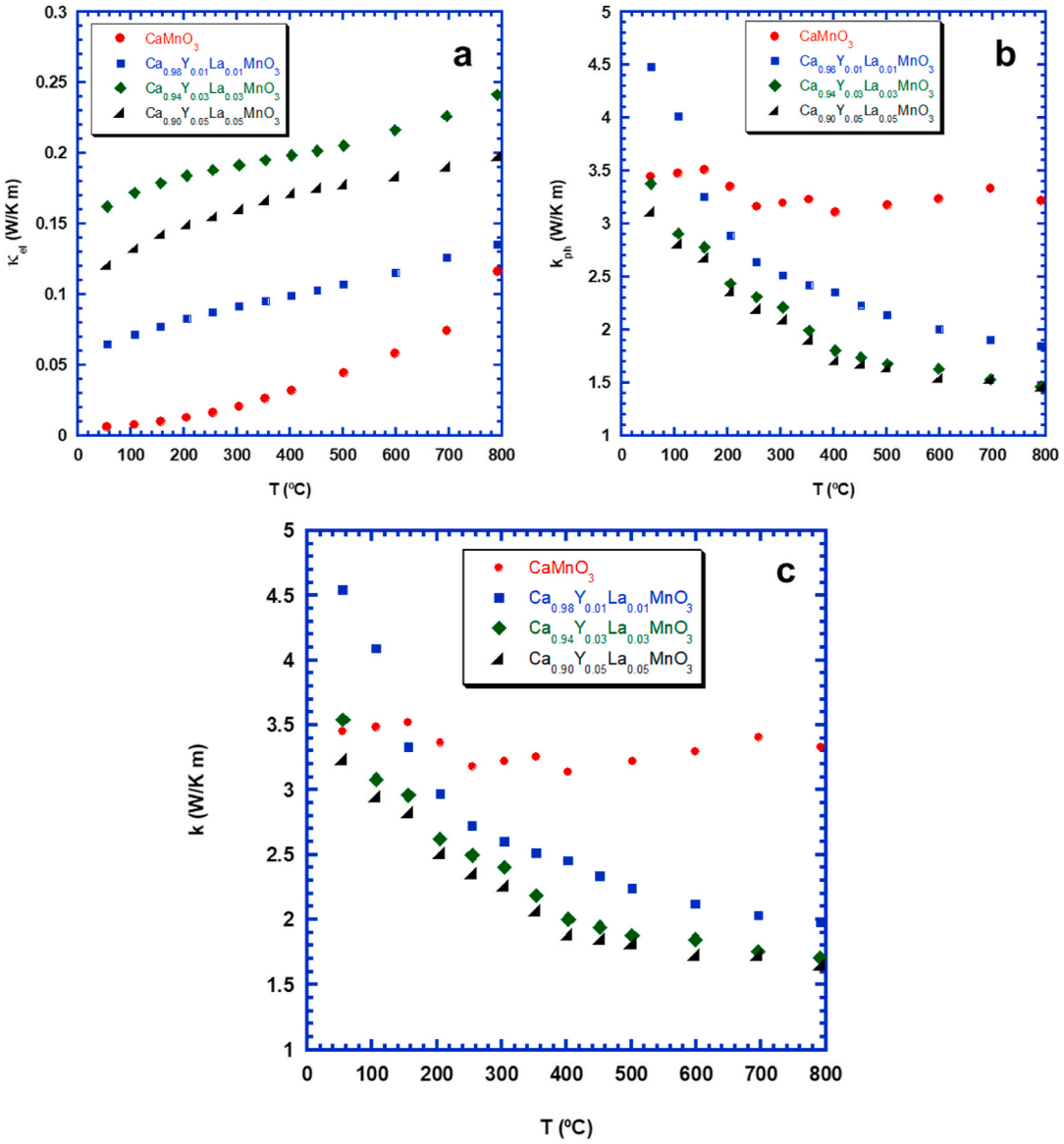

Fig. 7. a) Electronic; b) lattice and c) Total thermal conductivity variation with temperature as a function of the dopant content.

the crystalline cell parameters when the amount of dopant was raised. SEM studies denoted a decreasing trend of grain sizes when increasing dopant content. Moreover, very low amount of porosity is observed, leading to relative densities higher than 85 % of the theoretical ones of $CaMnO_3$ compound. Electrical resistivity significantly decreased with doping, when compared to the pristine sample, reflecting the increase in charge carrier concentration. The minimum values at 800 °C were measured in 0.03(Y, La)-doped samples (10.8 mΩ cm), which is within the typical values for this compound. Furthermore, the Seebeck coefficient followed the same trend, decreasing for higher dopant content, reaching the highest |S| value at 800 °C (300 μV/K) in 0.01(Y, La)-doped samples, which is much higher than the reported in the literature. The highest power factor at 800 °C (0.47 mW/K^2m) has been calculated in 0.01-doped samples provided by their very high S values and are among the best reported in the literature. On the other hand, despite their very large charge carrier concentration, the minimum thermal conductivity at 800 °C (1.65 W/K m) has been determined in 0.05-doped samples, being around the best reported in the literature, due to their smaller grain sizes, and the higher amount of high atomic weight cations. Finally, ZT values at 800 °C (0.25) are among the best values reported so far in this family of compounds. These results have been reached through the classical ceramic processing method and using lower amount of relatively cheap dopants than those typically reported in literature.

CRediT authorship contribution statement

P. Amirkhizi: Writing – review & editing, Writing – original draft, Methodology, Investigation, Formal analysis. **M.A. Madre:** Validation, Software, Formal analysis, Data curation. **O.J. Dura:** Writing – review & editing, Software, Formal analysis, Data curation. **M.A. Torres:** Software, Formal analysis, Data curation. **A. Sotelo:** Writing – review & editing, Writing – original draft, Validation, Supervision, Resources, Project administration, Conceptualization. **A.V. Kovalevsky:** Writing – review & editing, Supervision, Funding acquisition, Conceptualization. **Sh. Rasekh:** Writing – review & editing, Supervision, Funding acquisition, Conceptualization.

Declaration of competing interest

The authors declare that they have no known competing financial interests or personal relationships that could have appeared to influence

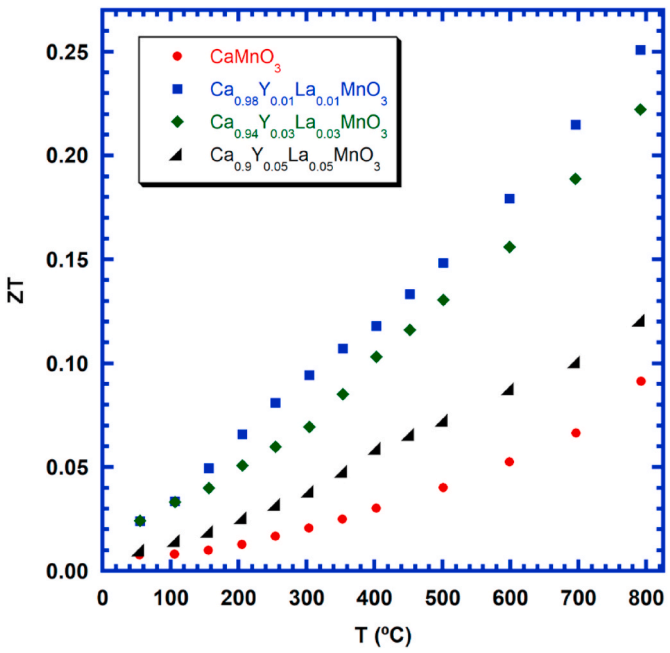

Fig. 8. ZT variation with temperature as a function of the dopant content.

the work reported in this paper.

Acknowledgements

The authors wish to thank the Gobierno de Aragón (Grupo de Investigacion T54_23R) and Universidad de Zaragoza (UZ2022-IAR-09) for financial support. Sh. Rasekh acknowledges the support of the Research Employment Contract FCT–CEECIND/02608/2017. This work was also developed within the scope of the PhD project of P. Amirkhizi (grant 2020.08051. BD funded by FCT) and the project CICECO-Aveiro Institute of Materials, UIDB/50011/2020, UIDP/50011/2020 & LA/P/0006/2020, financed by national funds through the FCT/MCTES (PIDDAC). M. A. Madre, M. A. Torres, and A. Sotelo acknowledge the grant CEX2023-001286-S funded by MICIU/AEI/10.13039/501100011033. Authors would like to acknowledge the use of Servicio General de Apoyo a la Investigación-SAI, Universidad de Zaragoza.

References

[1] S. Patidar, Applications of thermoelectric energy: a review, Int. J. Res. Appl. Sci. Eng. Technol. 6 (2018) 1992–1996, https://doi.org/10.22214/ijraset.2018.5325.
[2] M.A. Zoui, S. Bentouba, J.G. Stocholm, M. Bourouis, A review on thermoelectric generators: progress and applications, Energies 13 (2020) 3606, https://doi.org/10.3390/en13143606.
[3] D. Champier, Thermoelectric generators: a review of applications, Energy Convers. Manag. 140 (2017) 167–181, https://doi.org/10.1016/j.enconman.2017.02.070.
[4] D.M. Rowe, Thermoelectrics Handbook: Macro to Nano, first ed., CRC Press, Boca Raton, 2006.
[5] Tianyi Cao, Xiao-Lei Shi, Meng Li, Boxuan Hu, Wenyi Chen, Wei-Di Liu, Wanyu Lyu, Jennifer MacLeod, Zhi-Gang Chen, "Advances in bismuth-telluride-based thermoelectric devices: progress and challenges, eScience 3 (3) (2023) 100122, https://doi.org/10.1016/j.esci.2023.100122. ISSN 2667-1417.
[6] I.T. Witting, T.C. Chasapis, F. Ricci, M. Peters, N.A. Heinz, G. Hautier, G.J. Snyder, The thermoelectric properties of bismuth telluride, Adv. Electron. Mater. 5 (2019) 1800904, https://doi.org/10.1002/aelm.201800904.
[7] Pradeep Kumar Sharma, T.D. Senguttuvan, Vijay Kumar Sharma, Sujeet Chaudhary, "Revisiting the thermoelectric properties of lead telluride", Mater. Today Energy, Volume 21, 2021, 100713, ISSN 2468-6069, DOI: 10.1016/j.mtener.2021.100713.
[8] Ching-Hua Su, "Design, growth and characterization of PbTe-based thermoelectric materials, Prog. Cryst. Growth Char. Mater. 65 (2) (2019) 47–94, https://doi.org/10.1016/j.pcrysgrow.2019.04.001. ISSN 0960-8974.
[9] I. Terasaki, Introduction to thermoelectricity, in: C.C. Sorrell, S. Sugihara, J. Nowotny (Eds.), Materials for Energy Conversion Devices, Woodhead Publishing, 2005, pp. 339–357, https://doi.org/10.1533/9781845690815.3.339.
[10] A. Sotelo, P. Amirkhizi, O.J. Dura, G. García, A.C. Asensio, M.A. Torres, M. A. Madre, A. Kovalevsky, Sh Rasekh, Significant reduction in processing time for $Ca_{0.95}Ce_{0.05}MnO_3$ thermoelectric ceramics, Ceram. Int. 49 (2023) 37793–37799, https://doi.org/10.1016/j.ceramint.2023.09.107.
[11] I. Terasaki, Y. Sasago, K. Uchinokura, Large thermoelectric power in NaCo2O4 single crystals, Phys. Rev. B 56 (1997) R12685, https://doi.org/10.1103/PhysRevB.56.R12685.
[12] C. Li, Q. Chen, Y. Yan, Effects of Pr and Yb dual doping on the thermoelectric properties of CaMnO3, Materials 11 (2018) 1–13, https://doi.org/10.3390/ma11101807.
[13] D. Flahaut, T. Mihara, R. Funahashi, N. Nabeshima, K. Lee, H. Ohta, K. Koumoto, Thermoelectrical properties of A -site substituted $Ca_{1-x}Re_xMnO_3$ system, J. Appl. Phys. 100 (2006) 084911, https://doi.org/10.1063/1.2362922.
[14] S. Bresch, B. Mieller, F. Delorme, C. Chen, M. Bektas, R. Moos, T. Rabe, Influence of reaction-sintering and calcination conditions on thermoelectric properties of Sm-doped calcium manganate $CaMnO_3$, J. Ceram. Sci. Technol. 9 (2018) 289–300, https://doi.org/10.4416/JCST2018-00017.
[15] E. Ekstrom, A. le Febvrier, D. Fournier, J. Lu, V.-L. Ene, N.V. Nong, F. Eriksson, P. Eklund, B. Paul, Formation mechanism and thermoelectric properties of $CaMnO_3$ thin films synthesized by annealing of $Ca_{0.5}Mn_{0.5}O$ films, J. Mater. Sci. 54 (2019) 8482–8491, https://doi.org/10.1007/s10853-019-03496-7.
[16] Y.C. Zhou, C.L. Wang, W.B. Su, J. Liu, H.C. Wang, J.C. Li, Y. Li, J.Z. Zhai, Y. C. Zhang, L.M. Mei, Electrical properties of Dy^{3+}/Na^+ Co-doped oxide thermoelectric $[Ca_{1-x}(Na_{1/2}Dy_{1/2})_x]MnO_3$ ceramics, J. Alloys Compd. 680 (2016) 129–132, https://doi.org/10.1016/j.jallcom.2016.04.158.
[17] J.F. Shin, H. Niu, J. Alaria, J.B. Claridge, M.J. Rosseinsky, Substitution of Re^{7+} into $CaMnO_3$: an efficient free electron generation dopant for tuning of thermoelectric properties, Phys. Chem. Chem. Phys. 19 (2017) 30781–30789, https://doi.org/10.1039/c7cp06805k.
[18] K.R. Poeppelmeier, M.E. Leonowicz, J.C. Scanlon, B. Yelon, Structure determination of $CaMnO_3$, and $CaMnO_{2.5}$ by X-ray and neutron methods, J. Solid State Chem. 45 (1982) 71–79, https://doi.org/10.1016/0022-4596(82)90292-4.
[19] Q. Zhou, B.J. Kennedy, Thermal expansion and structure of orthorhombic $CaMnO_3$, J. Phys. Chem. Solid. 67 (2006) 1595–1598, https://doi.org/10.1016/j.jpcs.2006.02.011.
[20] C.S. Sanmathi, Y. Takahashi, D. Sawaki, Y. Klein, R. Retoux, I. Terasaki, J. G. Noudem, Microstructure control on thermoelectric properties of $Ca_{0.96}Sm_{0.04}MnO_3$ synthesised by co-precipitation technique, Mater. Res. Bull. 45 (2010) 558–563, https://doi.org/10.1016/j.materresbull.2010.01.023.
[21] J. Lan, Y.-H. Lin, H. Fang, A. Mei, C.-W. Nan, Y. Liu, S. Xu, M. Peters, High-temperature thermoelectric behaviors of fine-grained Gd-doped $CaMnO_3$ ceramics, J. Am. Ceram. Soc. 93 (2010) 2121–2124, https://doi.org/10.1111/j.1551-2916.2010.03673.x.
[22] H. Taguchi, T. Kugi, M. Kato, K. Hirota, Fabrication of $(Ca_{1-x}La_x)MnO_3$ ceramics with a high relative density and their power factor, J. Am. Ceram. Soc. 93 (2010) 3009–3011, https://doi.org/10.1111/j.1551-2916.2010.03987.x.
[23] R. Lohnert, M. Stelter, J. Topfer, Evaluation of soft chemistry methods to synthesize Gd-doped $CaMnO_{3-\delta}$ with improved thermoelectric properties, Mater. Sci. Eng. B 223 (2017) 185–193, https://doi.org/10.1016/j.mseb.2017.06.014.
[24] T. Liu, J. Chen, M. Li, G. Han, C. Liu, D. Zhou, J. Zou, Z.-G. Chen, L. Yang, Achieving enhanced thermoelectric performance of $Ca_{1-x-y}La_xSr_yMnO_3$ via synergistic carrier concentration optimization and chemical bond engineering, Chem. Eng. J. 408 (2021) 127364, https://doi.org/10.1016/j.cej.2020.127364.
[25] X. Li, L. Cui, J. Li, Y. Chen, W. Han, S. Shonkwiler, S. McMains, Automation of intercept method for grain size measurement: a topological skeleton approach, Mater. Des. 224 (2022) 111358, https://doi.org/10.1016/j.matdes.2022.111358.
[26] M.A. Madre, H. Amaveda, O.J. Dura, D. Pelloquin, M. Mora, M.A. Torres, S. Marinel, A. Sotelo, Effect of Y, La, and Yb simultaneous doping on the thermal conductivity and thermoelectric performances of $CaMnO_3$ ceramics, J. Alloys Compd. 954 (2023) 170201, https://doi.org/10.1016/j.jallcom.2023.170201.
[27] L. Rørmark, K. Wiik, S. Stølenb, T. Grande, Oxygen stoichiometry and structural properties of $La_{1-x}A_xMnO_{3\pm\delta}$ (A = Ca or Sr and $0 \leq x \leq 1$), J. Mater. Chem. 12 (2002) 1058–1067, https://doi.org/10.1039/b103510j.
[28] M. Molinari, D.A. Tompsett, S.C. Parker, F. Azough, R. Freerb, Structural, electronic and thermoelectric behaviour of $CaMnO_3$ and $CaMnO_{(3-\delta)}$, J. Mater. Chem. A 2 (2014) 14109, https://doi.org/10.1039/c4ta01514b.
[29] N. Kanas, B.A.D. Williamson, F. Steinbach, R. Hinterding, M.-A. Einarsrud, S. M. Selbach, A. Feldhoff, K. Wiik, Tuning the thermoelectric performance of $CaMnO_3$-based ceramics by controlled exsolution and microstructuring, ACS Appl. Energy Mater. 5 (2022) 12396–12407, https://doi.org/10.1021/acsaem.2c02012.
[30] A. Vijay, S.C. Prasanth, R. Jose, P. Vineetha, K.V. Saravanan, A study on the effects of La/Sm codoping on the structural and high temperature thermoelectric properties of n-type $CaMnO_{3-\delta}$ perovskite, Cryst. Res. Technol. 57 (2022) 2200041, https://doi.org/10.1002/crat.202200041.
[31] N.M. Ferreira, N.R. Neves, M.C. Ferro, M.A. Torres, M.A. Madre, F.M. Costa, A. Sotelo, A.V. Kovalevsky, Growth rate effects on the thermoelectric performance of $CaMnO_3$-based ceramics, J. Eur. Ceram. Soc. 39 (2019) 4184–4188, https://doi.org/10.1016/j.jeurceramsoc.2019.06.011.
[32] M. Mouyane, B. Itaalit, Flash Combustion Synthesis of electron doped-$CaMnO_3$ thermoelectric oxides, Powder Technol. 264 (2014) 71–77, https://doi.org/10.1016/j.powtec.2014.05.022.
[33] Y.-H. Zhu, W.-B. Su, J. Liu, Y.-C. Zhou, J. Li, X. Zhang, Y. Du, C.-L. Wang, Effects of Dy and Yb co-doping on thermoelectric properties of $CaMnO_3$ ceramics, Ceram. Int. 41 (2015) 1535–1539, https://doi.org/10.1016/j.ceramint.2014.09.089.

[34] S. Quetel-Weben, R. Retoux, J.G. Noudem, Thermoelectric $Ca_{0.9}Yb_{0.1}MnO_{3-\delta}$ grain growth controlled by spark plasma sintering, J. Eur. Ceram. Soc. 33 (2013) 1755–1762, https://doi.org/10.1016/j.jeurceramsoc.2013.02.003.

[35] R. Kabir, D. Wang, T. Zhang, R. Tian, R. Donelson, T.T. Tan, S. Li, Tunable thermoelectric properties of $Ca_{0.9}Yb_{0.1}MnO_3$ through controlling the particle size via ball mill processing, Ceram. Int. 40 (2014) 16701–16706, https://doi.org/10.1016/j.ceramint.2014.08.033.

[36] B. Zhang, A. Chang, Q. Zhao, H. Ye, Y. Wu, Synthesis and thermoelectric properties of Yb-doped $Ca_{0.9-x}Yb_xLa_{0.1}MnO_3$ ceramics, J. Electron. Mater. 43 (2014) 4048–4055, https://doi.org/10.1007/s11664-014-3326-8.

[37] H. Wang, C. Wang, Synthesis of Dy doped $Yb_{0.1}Ca_{0.9}MnO_3$ ceramics with a high relative density and their thermoelectric properties, Mater. Res. Bull. 47 (2012) 2252–2256, https://doi.org/10.1016/j.materresbull.2012.05.061.

[38] Y. Zhu, C. Wang, H. Wang, W. Su, J. Liu, J. Li, Influence of Dy/Bi dual doping on thermoelectric performance of $CaMnO_3$ ceramics, Mater. Chem. Phys. 144 (2014) 385–389, https://doi.org/10.1016/j.matchemphys.2014.01.006.

[39] D. Flahaut, J. Allouche, A. Sotelo, Sh Rasekh, M.A. Torres, M.A. Madre, J.C. Diez, Role of Ag in textured-annealed $Bi_2Ca_2Co_{1.7}O_x$ thermoelectric ceramic, Acta Mater. 102 (2016) 273–283, https://doi.org/10.1016/j.actamat.2015.09.036.

[40] K.K. Liu, Z.Y. Liu, F.P. Zhang, J.X. Zhang, X.Y. Yang, J.W. Zhang, J.L. Shi, G. Ren, T.W. He, J.J. Duan, Improved thermoelectric performance in Pr and Sr Co-doped $CaMnO_3$ materials, J. Alloys Compd. 808 (2019) 151476, https://doi.org/10.1016/j.jallcom.2019.07.188.

[41] R. Kabir, R. Tian, T. Zhang, R. Donelson, T.T. Tan, S. Li, Role of Bi doping in thermoelectric properties of $CaMnO_3$, J. Alloys Compd. 628 (2015) 347–351, https://doi.org/10.1016/j.jallcom.2014.12.141.

[42] M. Ohtaki, H. Koga, T. Tokunaga, K. Eguchi, H. Arai, Electrical transport properties and high-temperature thermoelectric performance of $(Ca_{0.9}M_{0.1})MnO_3$ (M= Y, La, Ce, Sm, In, Sn, Sb, Pb, Bi), J. Solid State Chem. 120 (1995) 105–111, https://doi.org/10.1006/jssc.1995.1384.

[43] T. Wang, P. Nan, H.C. Wang, W. Su, A. Sotelo, J. Zhai, X. Wang, Y. Ran, T. Chen, C. L. Wang, Right heterogeneous microstructure for achieving excellent thermoelectric performance in $Ca_{0.9}R_{0.1}MnO_{3-\delta}$ (R=Dy, Yb) ceramics, Inorg. Chem. 57 (2018) 9133–9141, https://doi.org/10.1021/acs.inorgchem.8b01163.

[44] G. Xu, R. Funahashi, I. Matsubara, M. Shikano, Y. Zhou, High-temperature thermoelectric properties of the $Ca_{1-x}Bi_xMnO_3$ system, J. Mater. Res. 17 (2002) 1092–1095, https://doi.org/10.1557/JMR.2002.0161.

[45] T. Chen, J. Wang, X. Wang, H. Wang, W. Su, J. Zhai, F. Mehmood, M. Khan, C. Wang, Cross-scale porous structure design leads to optimized thermoelectric performance and high output power for $CaMnO_3$ ceramics and their uni-leg modules, Appl. Mater. Today 29 (2022) 101557, https://doi.org/10.1016/j.apmt.2022.101557.

[46] Y. Wang, Y. Sui, W.H. Su, High temperature thermoelectric characteristics of $Ca_{0.9}R_{0.1}MnO_3$ (R = La, Pr, Yb), J. Appl. Phys. 104 (2008) 093703, https://doi.org/10.1063/1.3003065.

[47] Y. Wang, Y. Sui, H. Fan, X. Wang, W. Su, X. Liu, High temperature thermoelectric response of electron-doped $CaMnO_3$, Chem. Mater. 21 (2009) 4653–4660, https://doi.org/10.1021/cm901766y.

[48] A. Bhaskar, C. Liu, J. Yuan, Thermoelectric and magnetic properties of $Ca0.98Re0.02MnO_{3-\delta}$ (Re=Sm, Gd and Dy), J. Electron. Mater. 41 (2012) 2338–2344, https://doi.org/10.1007/s11664-012-2159-6.